Predictions of the effect of clumping on the wind properties of O-type stars

Muijres, L.E.; de Koter, A.; Vink, J.S.; Krticka, J.; Kubát, J.; Langer, N.

DOI
10.1051/0004-6361/201014290

Publication date
2011

Document Version
Final published version

Published in
Astronomy & Astrophysics

A&A 526, A32 (2011)
DOI: 10.1051/0004-6361/201014290

Astronomy & Astrophysics

Predictions of the effect of clumping on the wind properties of O-type stars

L. E. Muijres[1], A. de Koter[1,2], J. S. Vink[3], J. Krtička[4], J. Kubát[5], and N. Langer[6,2]

[1] Astronomical Institute "Anton Pannekoek", University of Amsterdam, PO Box 94249, 1090 GE Amsterdam, The Netherlands
e-mail: lmuijres@gmail.com
[2] Astronomical Institute, Utrecht University, Princetonplein 5, 3584 CC Utrecht, The Netherlands
[3] Armagh Observatory, College Hill, Armagh BT61 9DG, Northern Ireland, UK
[4] Department of Theoretical Physics and Astrophysics, Masaryk University, Kotlářská 2, 611 37 Brno, Czech Republic
[5] Astronomický ústav, Akademie věd České republiky, 251 65 Ondřejov, Czech Republic
[6] Argelander-Institut für Astronomie der Universität Bonn, Auf dem Hügel 71, 53121 Bonn, Germany

Received 19 February 2010 / Accepted 28 August 2010

ABSTRACT

Aims. Both empirical evidence and theoretical findings indicate that the stellar winds of massive early-type stars are inhomogeneous, i.e., porous and clumpy. For relatively dense winds, empirically derived mass-loss rates might be reconciled with predictions if these empirical rates are corrected for clumping. The predictions, however, do not account for structure in the wind. To allow for a consistent comparison, we investigate and quantify the effect of clumpiness and porosity of the outflow on the predicted wind energy and the maximal effect on the mass-loss rate of O-type stars.

Methods. Combining non-LTE model atmospheres and a Monte Carlo method to compute the transfer of momentum from the photons to the gas, the effect of clumping and porosity on the energy transferred from the radiation field to the wind is computed in outflows in which the clumping and porosity stratification is parameterized by heuristic prescriptions.

Results. The impact of structure in the outflow on the wind energy is complex and is a function of stellar temperature, the density of gas in the clumps, and the physical scale of the clumps. If the medium is already clumped in the photosphere, the emergent radiation field will be softer, slightly increasing the wind energy of relatively cool O stars (30 000 K) but slightly decreasing it for relatively hot O stars (40 000 K). More important is that as a result of recombination of the gas in a clumped wind the line force increases. However, because of porosity the line force decreases, simply because photons may travel in-between the clumps, avoiding interactions with the gas. If the changes in the wind energy only affect the mass-loss rate and not the terminal velocity of the flow, we find that the combined effect of clumpiness and porosity is a small reduction in the mass-loss rate if the clumps are smaller than 1/100th the local density scale height H_ρ. In this case, empirical mass-loss determinations based on Hα fitting and theory match for stars with dense winds ($\dot{M} \gtrsim 10^{-7}\ M_\odot\ \mathrm{yr}^{-1}$) if the overdensity of gas in the clumps, relative to the case of a smooth wind, is modest. For clumps larger than 1/10th H_ρ, the predicted mass-loss rates exhibit almost the same dependence on clumpiness as do empirical rates. We show that this implies that empirical and predicted mass-loss rates can no longer be matched. Very high overdensities of gas in clumps of such large size may cause the predicted $\dot{M}$ to decrease by a factor of from 10 to 100. This type of structure is likely not to be the cause of the "weak-wind problem" in early-type stars, unless a mechanism can be identified that causes extreme structure to develop in winds for which $\dot{M} \lesssim 10^{-7}\ M_\odot\ \mathrm{yr}^{-1}$ (weak winds) that is not active in denser winds.

Key words. radiative transfer – stars: early-type – stars: massive – stars: mass-loss – stars: winds, outflows

1. Introduction

In the last decade studies of the mass-loss rate of early-type massive stars have focused, for an important part, on the role of structure or inhomogeneities in the stellar outflow (for a review, see e.g. Puls et al. 2008). One reason is that recombination-based processes are very sensitive to the presence of structure in the wind and that therefore key mass-loss diagnostics, such as Hα and He II λ4686 line radiation and infrared and radio continuum radiation, which are sensitive to the square of the density, are affected. As a result, analyses based on these diagnostics assuming a smooth outflow will lead to an overestimate of the mass-loss rate if in reality the wind has a clumpy structure. One can show that if the typical clumping factor, expressing the ratio of the actual density in clumps relative to the mean density, is given by $C_\mathrm{c} > 1$, the empirical mass-loss rate $\dot{M}$ needs to be scaled down by a factor $1/\sqrt{C_\mathrm{c}}$ (see Sect. 2.2.1 for more details).

Attempts to empirically quantify the clumping factor in O stars, Luminous Blue Variables, and Wolf-Rayet stars yield a rather broad spectrum of C_c values, from a factor of a few up to 100 (see e.g. Figer et al. 2002; Crowther et al. 2002; Hillier et al. 2003; Bouret et al. 2003; Repolust et al. 2004; Markova et al. 2004; Bouret et al. 2005; Fullerton et al. 2006). This implies that empirical mass-loss rates may have to be scaled down by factors 2–10. To provide one explicit example, intended to serve as a frame of reference, empirical mass-loss rates of O-type stars brighter than 175 000 $L_\odot$ based on the analysis of Hα and assuming smooth flows are brought into agreement with predictions (Vink et al. 2001) if clumping is modest ($C_\mathrm{c} \sim 3$–4, Mokiem et al. 2007; de Koter et al. 2008). We note that recent stellar evolution calculations adopt these predictions, therefore,

if these predictions are correct, they account implicitly for a modest amount of clumping.

A second reason for the attention to this topic is that empirical studies of the radial stratification of the clumping factor throughout the wind portray a picture that disagrees with that is expected. Hydrodynamical modeling of the time-dependent structure of line-driven winds (for a review, see e.g. Owocki 1994; Feldmeier 1999) finds that the wind is quite stable in the inner parts, but predicts that extensive structure – in terms of both density and velocity – develops further out (at $r \gtrsim 1.3$ times the stellar radius $R_\star$ or $v \gtrsim 0.4$ times the terminal velocity) and can survive out to very large distances ($r \gtrsim 1000\ R_\star$, see Runacres & Owocki 2005). Empirical studies, however, show that O stars develop clumping already close to the stellar surface (Markova et al. 2004; Repolust et al. 2004; Puls et al. 2006). Apparently, the line-driven instability – first proposed by Lucy & Solomon (1970) – is not the only mechanism at work and other effects, acting in different parts of the wind, may also cause structure.

In this paper, we address the following question: does structure affect the rate at which massive stars lose mass? On the one hand, if structure were to cause the mass loss to increase, only modest clumping would be required to bring the above-mentioned Hα-based and predicted mass-loss rates into agreement. If, on the other hand, structure were to cause a strong decrease in $\dot{M}$, strong clumping would be required to ensure the above agreement or no agreement would be reached at all.

The hydrodynamic models of line-driven winds (see again Owocki 1994) predict that the time-averaged terminal flow velocity and time-averaged mass-loss rate agree well with those inferred from a stationary approach, i.e., there is no significant impact of clumping on either $\dot{M}$ or the terminal flow velocity v_∞. These predictions, however, are based on one-dimensional calculations (but see Dessart & Owocki 2003, 2005, for first results on two-dimensional flows), i.e., neglect a possible porous structure of the wind. In addition, the impact of the density and velocity perturbations on the excitation and ionization state of the gas, hence on the local line force, is not treated.

For certain aspects of this problem, we adopt a heuristic approach. We feel that this is justified because of both the discrepancies between the empirical clumping stratification and that predicted by the line-driven instability and the complex nature of the problem. We focus on the effects of clumping and porosity on changes in the state of the gas and the continuum radiation field, and on the impact of these changes on the line force. These effects are computed self-consistently. The clumping and porosity is, however, described by simple empirical laws. In Sect. 2, the method is described in detail. The results are presented in Sect. 3 and discussed in Sect. 4. We end with our conclusions.

2. Method

2.1. NLTE hydrodynamic wind models

To determine the momentum transfer from the radiation field to the wind in O-stars, we employ the model atmospheres of de Koter et al. (1993) in combination with a Monte Carlo code for determining the line force described by de Koter et al. (1997). The Monte Carlo approach, although extensively modified, is essentially based on that developed by Abbott & Lucy (1985). This methodology of determining the properties of stellar winds has been used extensively to predict the mass-loss behavior of massive early-type stars, including O and B stars (Vink et al. 1999, 2000, 2001), Luminous Blue Variables (Vink & de Koter 2002, LBVs), and selected Wolf-Rayet stars (de Koter et al. 1997; Vink & de Koter 2005). For details of the method, we refer the reader to the above references. Here, we provide only a brief overview of essential aspects.

The atmospheric model extends from the base of the photosphere (at a Rosseland optical depth of about 25) to 20 stellar radii, and assumes that the outflow is homogeneous, spherically symmetric, and stationary. To calculate the radiative transfer in spectral lines, the Sobolev method is used. The occupation numbers of (excited) levels and the ionization conditions are solved assuming statistical equilibrium. Model atoms for hydrogen, helium, carbon, nitrogen, oxygen, and silicon are explicitly treated. Other atoms are accounted for using a modified nebular approximation.

We emphasize that in our method the equation of motion for gas streaming out from the star is not solved explicitly (but see Müller & Vink 2008 and Muijres et al. 2010). We adopt, instead, a β-type velocity law. For this velocity structure, we compute, by means of Monte Carlo simulations, the total radial momentum that is transferred from photons to the gas on their way from the photosphere to the interstellar medium. The cumulative effect of this process also determines the total rate at which the wind extracts energy from the radiation field. By assuming that this energy is used to accelerate the wind and allow the gas to escape from the stellar potential well (hence that no non-radiative forces are at work), we can iteratively derive a mass-loss rate, given by

$$\Delta L = \frac{1}{2}\dot{M}\left(v_\infty^2 + v_{\rm esc}^2\right), \quad (1)$$

where ΔL is the energy extracted from the radiation field, v_∞ is the terminal wind velocity, and $v_{\rm esc}$ is the escape velocity from the stellar surface.

The advantages of this method are that mass-loss rates can be derived with a modest computational effort, hence relatively large fractions of parameter space can be explored. From a physical point, the strong point of the method is that the effects of multiple photon-scattering (that are already important for O stars) are self-consistently accounted for and that changes in the line force due to excitation/ionization processes are included. Our method predicts the gain in total kinetic energy of the outflow due to the transfer of momentum in the radiation field to the gas. This technique requires a pre-specified velocity law $v(r)$. Therefore, we do not predict the velocity stratification (nor the terminal flow velocity) but assume an empirically motivated $v(r)$. This allows us to extract the predicted mass-loss rate. In this study, we investigate the effects of clumping and porosity on the transferred energy ΔL, thus the wind energy. Since our velocity stratification is pre-specified, we cannot investigate the effects of structure on v_∞. Therefore, if one contributes the full effect of clumping and porosity to a change in the mass-loss rate, one obtains the maximal effect of these processes on $\dot{M}$.

2.2. The implementation of clumping

A self-consistent treatment of clumping in a stellar outflow would in any case require a hydrodynamical simulation of the line-driven instability (see e.g., Owocki & Puls 1999, and references therein) subject to a non-local thermodynamic (NLTE) treatment of the gas. From a computation point, this is extremely challenging. It is, moreover, currently unclear whether or not

the line-driven instability is the only process causing inhomogeneities in the outflow (see Sect. 2.2.1). For these reasons, we argue that a more heuristic approach to this problem is justified.

In our model, we prescribe the radial behavior of clumping assuming; *i)* all the gas is concentrated in clumps, i.e. the space in-between the clumps is void; *ii)* each clump is homogeneous; *iii)* clumps are distributed randomly on small spatial scales and follow a prescribed radial behavior on large spacial scales; and *iv)* the velocity law (of the clumpy medium) is a smooth function of radius.

The radial behavior of the clumping is prescribed in terms of the clumping factor, which indicates the overdensity in the clump relative to a smooth medium, and the porosity length, providing a physical scale of the clumps. We now introduce these two concepts in more detail.

2.2.1. Clumping factor

Following e.g. Owocki & Cohen (2006), we define the clumping factor to be

$$C_c(r) = \langle \rho(r)^2 \rangle / \langle \rho(r) \rangle^2, \tag{2}$$

where the angle brackets denote volume averaging. Empirical arguments motivated this definition. The strength of both the free-free continuum and the spectral lines formed by the process of recombination depend on the square of the density, while other processes, for instance that of electron scattering, exhibit a linear dependence (see e.g. Hillier 1991).

In an interclump medium that is void (see above), the density in the clump is given by

$$\rho_c(r) = C_c(r) \langle \rho(r) \rangle. \tag{3}$$

The simplest possible assumption about the behavior of clumping is that it is 1) constant throughout the photosphere and wind and equal to $C_c > 1$. A clumping factor of $C_c = 1$ corresponds to a smooth wind. To investigate a radial dependence in the clumping, we introduce additional clumping prescriptions. A schematic representation of all clumping stratifications adopted in this study is given in Fig. 1. The top drawing (labeled 1) depicts the case of a constant clumping factor.

Clumping in the outer wind. In this prescription, we assume that the onset of clumping occurs at some prescribed radius r_p, i.e.

$$C_c(r) = \begin{cases} 1.0 & \text{for} \quad r < r_p, \\ C_c & \text{for} \quad r \geq r_p. \end{cases} \tag{4}$$

The onset and development of stochastic structure in the acceleration zone of the outflow is a natural consequence of a line-driven wind. It is the result of a positive feedback in which a small increase in the velocity of a fluid parcel exposes the parcel to more intense, unattenuated radiation from the star and causes it to be further accelerated (Owocki et al. 1988; Feldmeier 1995; Owocki & Puls 1996, 1999). Simulations of this *self-excited* wind instability show that the gas compression in clumps typically starts at about 0.3–0.4 v_∞ and can extend to very large radii (Runacres & Owocki 2002). These simulations, however, do not account for (transonic) velocity curvature terms. In stars with relatively weak winds, it has been shown that these terms may lead to gradient terms in the source function and modifications of the line acceleration (Puls et al. 1998) causing a highly structured wind in the lower parts of the outflow

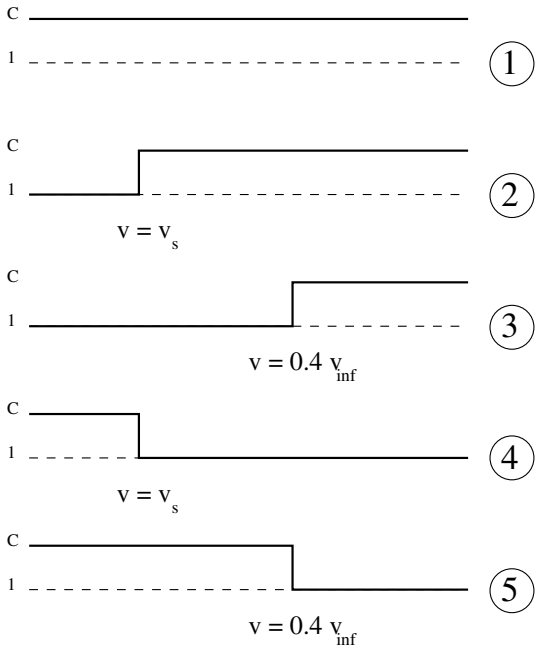

Fig. 1. Schematic representation of the different clumping stratifications investigated in this study. Each stratification has been given an index number (at the right side of the figure), which is used in Fig. 4. They represent (1) constant clumping, (2) clumping starting at the sonic point, (3) clumping starting at 0.4 v_∞, (4) clumping up to the sonic point, and (5) clumping up to 0.4 v_∞.

(Owocki & Puls 1999). The theory of line driven winds dictates that the mass-loss rate is set by conditions at or below a critical point that is very roughly at 0.2 v_∞.

On the basis of the above arguments for structure formation in line-driven winds, we define two additional clumping prescriptions, where we opt to initiate the clumping: 2) at the sonic velocity (about 15 km s^{-1} for the models of 30 kK and about 18 km s^{-1} for the models of 40 kK), and 3) at 0.4 v_∞ (see Table 1 for values of v_∞). The former clumping stratification explores a potential effect of clumping on the mass-loss rate because clumping sets in before the mass-loss rate is formally fixed. The latter prescription focusses on the effect of clumping on v_∞ (see again Fig. 1). The density in the clumps produced by the line-driven instability relative to the ambient medium can reach one to two orders of magnitude (Owocki & Puls 1999). We adopt clumping factors C_c of unity through to 100, in steps of 0.5 dex.

Clumping in the inner wind. In this prescription, we assume that clumping occurs in the inner wind and that the outer wind is smooth, i.e.

$$C_c(r) = \begin{cases} C_c & \text{for} \quad r < r_p, \\ 1.0 & \text{for} \quad r \geq r_p, \end{cases} \tag{5}$$

where r_p again refers to the prescribed radius defining the boundary between the two regimes. This clumping prescription is the "opposite" of that described in the previous paragraph, which was motivated by theoretical expectations. The clumping prescription of Eq. (5) is motivated by observational arguments. Puls et al. (2006) present empirical evidence for a radial dependence of clumping in hot star winds. These authors use Hα, infrared and radio diagnostics to investigate the clumping behavior of the inner wind (within about two stellar radii) relative to the clumping in the outer wind (beyond tens of stellar radii) of a

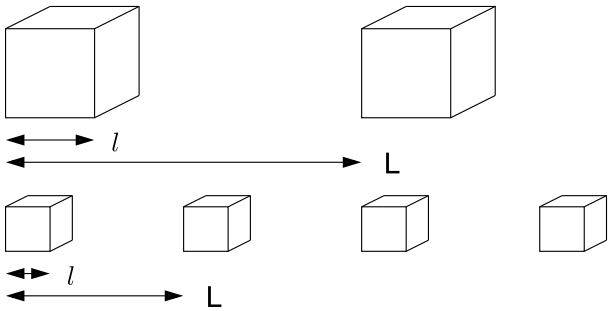

Fig. 2. Schematic explanation of the difference between the filling fraction f, c.q. clumping factor $C_c = 1/f$, which is the same for the top and bottom case, and the separation of the clumps L, which is larger in the top case.

large sample of giant and supergiant stars. They find a qualitative difference in the radial behavior of clumping in stars with strong winds compared to stars with weak winds. In the case of dense winds, the inner wind is *more strongly* clumped than the outer wind, whereas in the case of thin winds the inner and outer region have similar clumping properties. Puls et al. speculate that the cause of this difference between strong and weak winds may be related to photospheric instabilities and/or pulsations as their strong wind stars are usually supergiants with low gravity. Interestingly, Cantiello et al. (2009) demonstrate that the stars studied by Puls et al. that have stronger clumping in the inner wind than in the outer wind have sub-surface convective layers due to iron opacity peaks. They suggest that this convection may (indirectly) trigger stochastic velocities and clumping in the photosphere and lower part of the wind.

On the basis of these arguments, we again define two clumping stratifications: 4) clumping up to the sonic point, and 5) clumping up to 0.4 v_∞ (see also Fig. 1).

2.2.2. Porosity length

If the physical scale of a clump is given by ℓ and the separation of clumps by L (see Fig. 2 for a visualization of the definition of L), a fraction $f = \ell^3/L^3$ of the medium will be filled with gas, again assuming that the inter-clumped medium is void. This filling fraction f relates to the clumping factor as $C_c = 1/f$. In Fig. 2, two possible configurations of regularly stacked cubic clumps with identical filling fractions f (and clumping factors C_c) are shown. The way in which these configurations differ is in the physical size and separation of the clumps. If in both configurations the individual clumps are optically thin to radiation, the effects of clumping will be the same and only occur by an adjustment of the excitation and ionization properties of the gas. If, however, the physical size of the large clumps is such that the individual clumps become optically thick, they will be affected by from local self-shielding. In this case, the medium becomes *porous*, i.e. radiation will be able to travel more efficiently through inter-clump channels. The longer the scale length L, the more efficient this mechanism will be (for instance, when all material in the outflow is concentrated in a single clump). Porosity in stellar winds, sometimes referred to as macro-clumping, is discussed by Feldmeier et al. (2003), Owocki et al. (2004), Owocki & Cohen (2006), and Oskinova et al. (2007).

The effective opacity of a clump is given by

$$\kappa_{\rm eff} = \kappa_c(\rho_c)\,\frac{1-\exp(\tau_c)}{\tau_c}, \tag{6}$$

where $\kappa_{\rm eff}$ is the effective mass absorption coefficient (e.g. in cm^2 gr^{-1}) of an ensemble of clumps. The mass absorption coefficient of material in the clumps, κ_c, is thus reduced because of the porous nature of the medium. The clump optical thickness $\tau_c = \kappa_c\,\rho_c\,\ell = \kappa_c\,C_c\langle\rho\rangle\,\ell = \kappa_c\,\langle\rho\rangle\,\ell/f$.

We introduce a radial dependence of the scale of the clumps, i.e.

$$L(r) = \begin{cases} \text{negligible} & \text{for} \quad r < r_p, \\ H_\rho/D & \text{for} \quad r \geq r_p, \end{cases} \tag{7}$$

where H_ρ is the local density scale height and D is a constant, which we choose to be 10, 100, and 1000. That L is negligible below r_s implies that we do not account for porosity in the subsonic part of the outflow. The increase in the physical scale $\ell = L\,C_c^{-1/3}$ with radial distance reflects the likely case in which the clumps expand and possibly merge while receding from the star.

To provide a quantitative feeling for the number of clumps, we compute the number of clumps N passing a radial shell at r in a typical flow time $\tau = R_\star/v_\infty$. We define this as the total volume associated with one wind flow time divided by the volume in which there is one clump. One finds that

$$N = 4\pi r^2 \left(\frac{D}{H_\rho}\right)^3 \frac{R_\star}{v_\infty}\,v(r). \tag{8}$$

In our dwarf model of 30 000 K, the scale height has increased to about half a stellar radius at $r = 2\,R_\star$. At this point, the flow velocity is 1100 km s^{-1}. For N, we find that $\sim 200 D^3$. We note that the number of clumps is not conserved, but decreases with distance. For instance, in the same model $H_\rho \sim 0.1\,R_\star$ at $r = 1.1\,R_\star$, therefore the number of clumps passing this point in one flow time is about 3.5 times as large as that at $r = 2\,R_\star$. Physically, this implies that in our description clumps merge as they move away from the surface.

2.2.3. Vorosity

The velocity law of the structured medium is assumed to be as a monotonic function of radius. We therefore do not assume that on a local scale (where the flow speed is almost constant) an ensemble of clumps may have a range in velocities, nor do we account for shape changes of individual clumps caused by internal velocity gradients. The overlaps and/or gaps in velocity space that may be produced by these motions are termed "vorosity" (which is short for velocity porosity). A general treatment of vorosity is beyond the scope of this study. We point out, however, that the intrinsic instability of the line-driving mechanism is expected to lead to velocity structure. Assuming that the internal velocity dispersion in a clump is small, and that clump velocities sample the smooth outflow (matter being concentrated in the clumps), Owocki (2008), adopting one-dimensional dynamical simulations of the wind instability, finds a reduction in the over-all line absorption of about 10–20%. In our simulations, the velocity change inside a single clump is treated in essentially a similar way as in Owocki. It is assumed to be monotonic and amounts to $\delta v \sim (\mathrm{d}v/\mathrm{d}s) \times \ell$, where s is the geometrical distance in the arbitrary direction s and v is the smooth flow velocity. The value of δv is typically small.

Radiation hydrodynamical simulations (in 2D) exhibit, however, a large velocity dispersion in the clumps (Sundqvist et al. 2010). Interestingly, Sundqvist et al. point out that this structure prevents a desaturation of lines (of intermediate strength) also implying only a modest reduction in the line absorption.

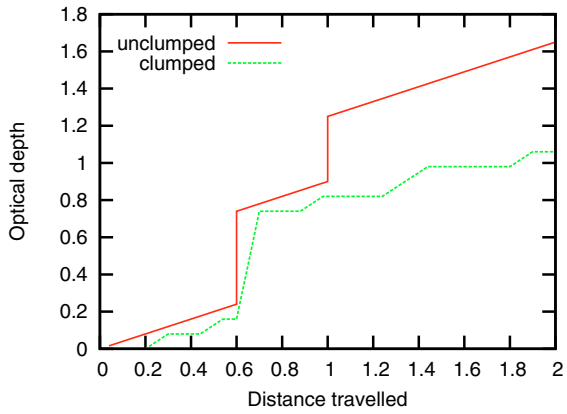

Fig. 3. Schematic representation of the increase in optical depth with distance. The latter is given in arbitrary units. The slope of the lines thus represent the linear extinction coefficient $\kappa\rho$. The solid line depicts the case of a smooth medium; the dashed line that of a clumpy medium. In the smooth flow, the slanted regions represent continuum extinction, while at the points where the line becomes vertical a line interaction occurs. The line interaction region is assumed to be infinitely narrow. In the case of a clumpy flow, the flat parts of the curve reflect the inter-clump medium. Within a clump, the continuum extinction is relatively large, therefore the slope is relatively steep. For reasons explained in the text, we have assumed the line interaction region to have a finite width, determined by the Sobolev length. The line that can interact at about distance 1 is missed as it is associated with the inter-clump medium. We note that in a clumpy medium the photon needs to travel a larger geometrical depth to cross a given optical depth.

2.3. Inclusion of clumps in the Monte Carlo code

The mass-loss prediction consists of two parts. First, an ISA-WIND non-LTE spherically symmetric model atmosphere with prescribed outflow properties is computed. The atomic models and non-LTE treatment are identical to those of Vink et al. (2000). The density, casu quo velocity stratification, in the photosphere and the onset region of the wind is computed accounting by for the force due to the gradient in gas pressure and continuum radiation pressure. Near the sonic point, the velocity stratification is smoothly connected to a β-law. For details, we also refer to Vink et al. (2000). Clumping in the model atmosphere is implemented by means of the clumping factor $C_c(r)$ in the description of the density, Eq. (3). In the description of the optical depth, the clumping is treated in the effective opacity, Eq. (6), and the scale length, Eq. (7).

By neglecting the porosity correction in describing the opacity (in both ISA-WIND and MC-WIND), we can single out the effect of clumping on the excitation and ionization structure. We study the impact of clumping on the state of the gas in Sect. 3.1.

Second, the Monte Carlo simulation program MC-WIND is used to trace the momentum transfer of photons to the gas, from which a mass-loss rate can be derived following the method of Abbott & Lucy (1985). To study the full effect of clumping, the porous nature of the medium needs to be accounted for.

In a homogeneous medium without spectral lines, a photon traveling an optical depth $\Delta\tau_\nu$ will cross a geometrical distance $s = \Delta\tau_\nu/\kappa_\nu\rho$. In a spherically symmetric stellar wind with a monotonically increasing wind velocity in which both continuum and line absorption may occur, the photon will experience a local barrier in optical depth at regions where its frequency matches that of a spectral line. If we map the distance in optical depth to a distance in physical space, one can reproduce the behavior schematically shown in Fig. 3. The figure depicts the situation in a spherical shell in which the density is assumed to be constant. The optical depth increases linearly with distance because of free-free processes, bound-free processes, and Thomson scattering. These are represented by the slanted parts of the line. In a rapidly expanding spherical outflow, a photon that is emitted at a wavelength slightly bluer than the wavelengths at which a spectral line may absorb, may interact with the spectral line once it encounters particles that move with the proper relative Doppler (red)shift. Assuming the typical width of the line is given by the Doppler width, $v_D = \sqrt{kT/m}$, where T is the temperature, k the Boltzmann constant, and m the mass of the particle, the geometrical length of a line absorption region is $L_{Sob} = v_D/(dv/dz)$, where z measures the distance in the direction in which the photon is propagating. This length is referred to as the Sobolev length (Sobolev 1960). If the direction measured by z is at an angle θ with the radial direction, such that $\hat{z}/\hat{r} = \cos\theta = \mu$, then

$$\frac{dv}{dz} = \left(1-\mu^2\right)\frac{v}{r} + \mu^2\frac{dv}{dr}\,. \tag{9}$$

In computing the radiation field in spectral lines, the Sobolev approximation is adopted in ISA-WIND, i.e., it is assumed that the velocity gradient is so large that the properties of the medium do not change within a length interval L_{Sob}. In MC-WIND models without clumping, we assume that line interactions take place at the line center, i.e., the Sobolev absorption region is assumed to be infinitely narrow. The vertical solid lines in Fig. 3 reflect these line interactions, and represent an optical depth $\tau_{lu} = \kappa_{lu}\,\rho\,\lambda_{lu}\,L_{Sob}/v_D$. In this equation, the mass absorption coefficient of the transition at wavelength λ_{lu} between lower level l and upper level u is given by

$$\kappa_{lu} = \frac{\pi e^2}{m_e c} f_{lu}\frac{n_l}{\rho}\left(1-\frac{n_u}{n_l}\frac{g_l}{g_u}\right), \tag{10}$$

where e and m_e are the charge and mass of the electron, c the speed of light, f_{lu} is the oscillator strength, n_l and n_u the number densities of the lower and upper level, and g_l and g_u are the statistical weights of the lower and upper level. In the Monte Carlo simulation, the optical depth at which the photon should interact is randomly drawn and given by $\tau_\nu = -\ln p$, where $p \in \langle 0, 1]$ is a random number.

In a clumpy wind with a clumping factor C_c and porosity length L, photons travel alternatively through clumps and vacuum. If we assumed the Sobolev length L_{Sob} to be infinitely small, photons would "miss" spectral lines for which the interaction point is in a void region. If the interaction region were the actual Sobolev length, a fraction of these ineffective lines could still contribute to the opacity as part of the interaction region may coincide with the location of one or more nearby clumps. Accounting for the extent of the Sobolev interaction region yields a more representative sampling of the spectral lines contributing to the line force. For this reason, we account for the actual L_{Sob} by introducing a mean line opacity in the line interaction region

$$\chi_{lu} = \frac{\tau_{lu}}{L_{Sob}}\,. \tag{11}$$

This implies that we assume the line profile function to be a box function. The situation of a clumpy medium is depicted in Fig. 3 using a dashed line. When the dashed line is flat, the photon does not encounter any material. If the randomly selected optical depth the photon will travel is within the Sobolev region of one (or more) lines, a random selection, using the opacities

Table 1. Adopted model parameters and predicted mass-loss rates for all clumping assumptions.

$T_{\rm eff}$ (K)	R [$R_\odot$]	$\log L$ [$L_\odot$]	M [$M_\odot$]	v_∞ [km s^{-1}]	$\log C_{\rm c}$	log $\dot{M}$ [$M_\odot$ yr^{-1}] $C_{\rm c}$ constant	$C_{\rm c}$ from $v_{\rm s}$	$C_{\rm c}$ from 0.4 v_∞	$C_{\rm c}$ up to $v_{\rm s}$	$C_{\rm c}$ up to 0.4 v_∞
Dwarfs										
30 000	6.6	4.50	12.9	2176	0.0	–7.67	–7.67	–7.67	–7.67	–7.67
					0.5	–7.60	–7.64	–7.64	–7.63	–7.62
					1.0	–7.53	–7.56	–7.57	–7.63	–7.62
					1.5	–7.24	–7.32	–7.36	–7.56	–7.55
					2.0	–6.93	–7.01	–7.05	–7.58	–7.53
40 000	10.7	5.42	34.6	2585	0.0	–6.13	–6.13	–6.13	–6.13	–6.13
					0.5	–6.11	–6.00	–6.00	–6.21	–6.21
					1.0	–6.04	–5.93	–5.92	–6.23	–6.23
					1.5	–5.99	–5.86	–5.82	–6.24	–6.22
					2.0	–5.84	–5.78	–5.72	–6.27	–6.23
Supergiants										
30 000	22.4	5.56	28.8	1506	0.0	–5.90	–5.90	–5.90	–5.90	–5.90
					0.5	–5.73	–5.80	–5.78	–5.93	–5.91
					1.0	–5.33	–5.54	–5.57	–5.87	–5.80
					1.5	–5.14	–5.23	–5.30	–5.88	–5.72
					2.0	–4.94	–4.99	–5.03	–5.85	–5.56
40 000	19.1	5.93	58.1	2212	0.0	–5.22	–5.22	–5.22	–5.22	–5.22
					0.5	–5.21	–5.12	–5.11	–5.31	–5.29
					1.0	–5.20	–5.05	–5.00	–5.36	–5.36
					1.5	–5.19	–5.08	–4.90	–5.42	–5.43
					2.0	–5.10	–5.04	–4.84	–5.42	–5.46

Notes. Porosity is not included in these predictions, i.e., the clumps are assumed to be optically thin. We emphasize that the mass-loss rates given here have been calculated assuming that all of the change in wind energy contributes to $\dot{M}$. However, e.g. in the case in which clumping sets in at 0.4 v_∞ this is unlikely and most of the change contributes to v_∞.

of the contributing extinction processes at the point of interaction as a weighing factor, will determine the type of interaction. The outcome of this random process can be either a free-free or bound-free interaction, an electron scattering, or a line interaction.

The clumps themselves are assumed to be cubes, of which the length of the edge is $\ell = L/C_{\rm c}^{1/3}$. As explained, each volume L^3 contains a clump. The probability that a photon traveling this volume encounters a clump is given by the cross-section of the clump relative to the cross-section of the volume, i.e. $\ell^2/L^2 = C_{\rm c}^{-2/3}$. The clumps are randomly placed along the path of the photon using this probability.

On average, because of the effect of porosity and part of the lines becoming ineffective (i.e. those lines that have their line interaction region completely or partially in the inter-clump medium), photons need to travel a larger geometrical distance in a clumpy medium before being absorbed. Therefore, the dashed line in Fig. 3 is drawn such that it falls below the solid line. If a packet of photons interacts with material in a clump, it will be re-emitted in a random direction. For this new direction, we account for the photon packet starting in a clump.

2.4. Model grid

To study the effects of clumping and porosity, we defined a small grid of main-sequence stars and supergiants. The input parameters are listed in Table 1. To facilitate a comparison with the results of Vink et al. (2000), we adopted their solar abundance pattern, which follows Anders & Grevesse (1989). We note that applying the solar abundances of Asplund et al. (2005) would result in a typical reduction in the mass loss rate of 0.1 dex (see Krtička & Kubát 2007). Though the mass-loss rate is calculated, the velocity stratification is prescribed (see Sect. 2.1). We adopt a terminal velocity v_∞ that is 2.6 times the effective surface escape velocity, where "effective" implies that the surface gravity is corrected for radiation pressure on free electrons. The parameter β describing the rate of acceleration of the flow is set to unity. This is again similar to Vink et al. (2000). Theoretical support for this choice is given by Müller & Vink (2008).

For our five different clumping stratifications, the predicted mass-loss rates are given, each time for five different clumping factors. These results are discussed in the next section.

3. Results

3.1. The effect of clumping on M inferred from its impact on the photospheric radiation field and ionization of the gas

In Fig. 4, we show the predicted wind energies $E_{\rm kin} = 1/2\, \dot{M}\, v_\infty^2$ as a function of both the clumping prescription and clumping factor for two typical main-sequence stars (top panels) and two typical supergiants (bottom panels). $E_{\rm kin}$ has the dimensions of energy per unit time. The reason why we discuss the results in terms of $E_{\rm kin}$ and not in terms of $\dot{M}$ is that our Monte Carlo calculation essentially predicts the change in kinetic energy (see Sect. 2.1), but does not predict the effect on the velocity structure. If, in presenting the results, we assume that the terminal velocity is not affected[1], the effect of clumping can be expressed as a (change in) mass loss rate. This most certainly is not appropriate when clumping starts at 0.4 v_∞. It is to be expected that only when clumping has developed near the sonic point does the above assumption have merit. Hence, although we are unable to distinguish the effects on $\dot{M}$ and v_∞, we still opt to present changes in $\dot{M}$ only in all clumping prescription in Table 1 (and

[1] We note that this neglects the possibility of feedback, i.e. a fully consistent hydrodynamical treatment of clumping might in principle result in a complex reaction that does not obey $\Delta\dot{M} \propto \Delta v_\infty^{-2}$ for a given ΔL.

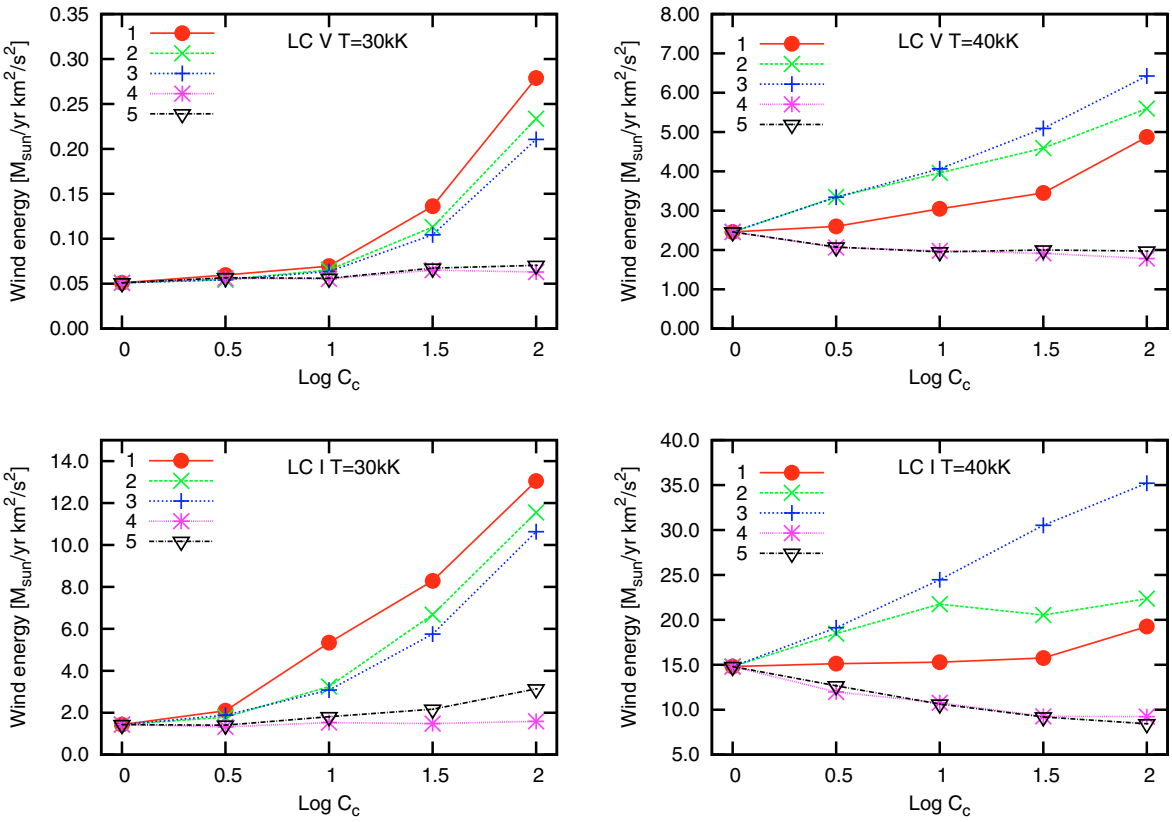

Fig. 4. Wind energy predictions for different clumping stratifications of selected O-type stars. The smooth wind models have $C_c = 1$. The numbers refer to those used in Fig. 1 to identify the clumping behavior. Clumping in the outer winds (stratifications 1 through 3) results in an increase of E_{kin} because of a higher number of effective driving lines. The effect of clumping on the photospheric spectrum (which occurs in stratifications 1, 4, and 5) is temperature dependent; for the 30 000 K (40 000 K) model, it leads to an increase (decrease) in $\dot{M}$. See Sect. 3.1 for a discussion.

also in Table 2). However, in the discussion Sect. 4 we will concentrate on the physically most relevant cases.

As explained in Sect. 2.4, the first four columns of Table 1 list stellar parameters and the fifth the adopted terminal velocity. In Col. 6, we indicate the clumping factor used in five different clumping prescriptions: constant clumping (Col. 7; filled red circles in the plot); clumping starting at the sonic point (Col. 8; green crosses) and at 0.4 v_∞ (Col. 9; blue plus symbols); and clumping in the photosphere and lower part of the wind up to the sonic point (Col. 10; purple crosses) and up to 0.4 v_∞ (Col. 11; black triangles). In these predictions, porosity is not included, which implies that we assume the clumps to be optically thin.

Clumping introduces two effects that impact the mass loss of the star. First, if clumping occurs in the stellar photosphere, the higher continuum opacity will shift the layer of continuum formation to lower temperatures, i.e. soften the radiation field. As a result, the Lyman and He I continuum flux will decrease, while the Balmer continuum flux increases. For a 30 000 K star, the wind driving relies strongly on the contribution of Fe IV, with Fe III supplying a non-negligible part. As the lines of these ions tend to cluster in the Balmer continuum, clumping in the photosphere will result in an increase in the mass-loss rate. For a 40 000 K star, the wind driving relies on Fe V and Fe IV lines (as well as on lines of carbon, nitrogen, and oxygen), preferentially located in the Lyman and He I continuum. In this case, clumping in the photosphere will therefore slightly lower the mass-loss rate. Second, clumping in the stellar wind will push the ionization balance of the wind driving ions towards a lower ionization stage. As shown by Vink et al. (1999), a dramatic increase in the mass loss rate is expected when iron recombines from Fe IV to Fe III near the sonic point. This occurs at ~25 000 K in a smooth wind and is referred to as the bi-stability jump. Though Fe III does not become dominant in even the most clumped winds (i.e. $C_c = 100$) of our 30 000 K star, the Fe III contribution does increase very substantially for large clumping factors causing a higher mass-loss. For the 40 000 K star, the increased importance of Fe IV relative to Fe V (and e.g. C III and C IV relative to C V) in a clumped outflow also has a positive effect on $\dot{M}$, though not as pronounced as in the 30 000 K star.

These considerations allow us to interpret the results in Fig. 4. In the 30 000 K stars, both the effect of clumping on the photospheric radiation field and the ionization balance work in the direction of an increase in the mass-loss rate (see also Gräfener & Hamann 2008). The small effect on $\dot{M}$ in clumping prescriptions 4 and 5, which both have clumping in the photosphere but not in the outer wind, shows that for this model the impact of clumping on the photospheric radiation field is negligible. The other three clumping prescriptions, 1, 2, and 3, demonstrate the importance of clumping in the outer wind. The situation of omnipresent clumping (prescription 1) is the most extreme. Here the mass loss may increase by up to a factor of 3 for $C_c = 10$ and 7 for $C_c = 100$. We note that if clumping is only modest ($C_c \lesssim 3$) only small changes in the mass-loss are expected.

The situation for the 40 000 K stars is slightly different. Here the two effects of clumping – the softening of the radiation field and the recombination of the gas – work in opposite directions. In clumping prescriptions 4 and 5, the impact of clumping on the

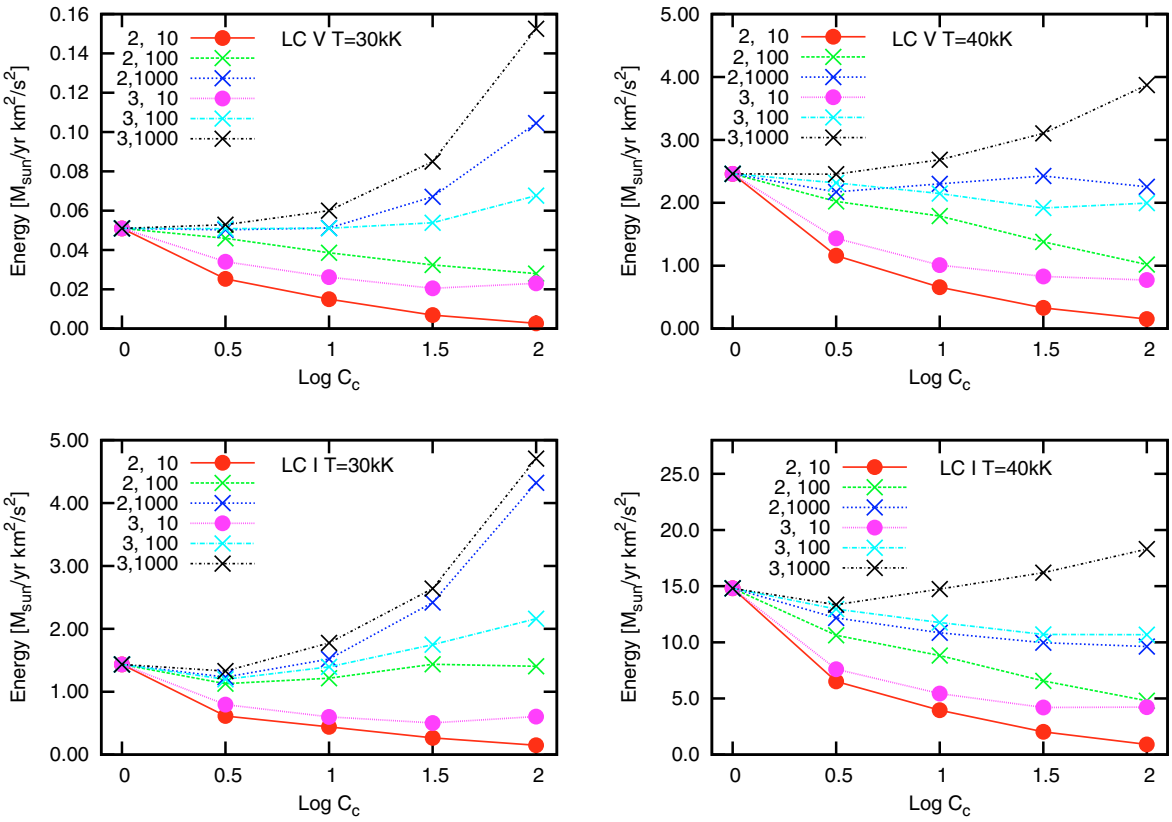

Fig. 5. Wind energy predictions accounting for both clumping *and* porosity of the clumping stratification in which clumping sets in at the sonic velocity (models labeled 2) and at 0.4 v_∞ (models labeled 3). The scale of the clumps is given by H_ρ/D, where $D = 10, 100, 1000$. These results should be compared to the corresponding models in Fig. 4, which account for clumping but not for porosity. The addition of porosity always causes a decrease in $E_{\rm kin}$. See Sect. 3.2 for a discussion.

photospheric spectrum causes a modest decrease in the mass loss (less than a factor of two for even the most extreme clumping). Clumping in the outer wind has the reverse effect, which is now most prominent in clumping prescriptions 2 and 3, which have no clumping in the photosphere. As prescription 1 has clumping everywhere, this model, unlike the 30 000 K case, now falls in-between 2 and 3, and 4 and 5. For the strongest clumping, the most extreme effect is found for prescription 2, though here the increase in mass loss is only about a factor of two. We note that modest clumping ($C_c \lesssim 3$) has about a 30% effect on $\dot{M}$.

3.2. The effect of porosity on M

The results that we have presented so far, assume that the clumps are optically thin. Now, we account for the actual optical depth of the clumps. This may cause the medium to become porous. To do so, we have to introduce the physical scale of the separation of the clumps L, as introduced in Sect. 2.2.2. The results in this case are given in Table 2. In Fig. 5, we show the effect of porosity for the case that clumping sets in at the sonic point (i.e. model 2 in Fig. 4) and at 0.4 v_∞ (model 3). The separation between the clumps is either 1/10, 1/100, or 1/1000 of the local scaleheight, i.e., $D = 10$, 100, or 1000. Though it seems reasonable to assume that such separations may develop in the wind, these rather large separations (small values of D) are very unlikely to occur in the stellar photosphere. For this reason, we focus on models 2 and 3.

In interpreting the results, it is important to realize that one should compare these to the predicted mass-loss rates shown in Fig. 4 for the relevant clumping factor, and not to the model that has a homogeneous outflow. Only by means of this comparison can one distinguish the effect of porosity on $\dot{M}$. It is clear that if the separation between the clumps is large (D is small), the effect of porosity will be strongest. Photons may travel relatively undisturbed through the interclump medium, avoiding interactions with the gas. For the extreme case $D = 10$, the drop in $\dot{M}$ due to the geometrical effect of porosity may be as large as one to two orders of magnitude. For $D = 1000$, the drop is at most a factor of three. The impact of porosity is less severe if clumping sets in farther out in the wind, as expected.

As an example of the quantitative behavior, we consider a model where clumping sets in at the sonic point and $C_c = 100$. The drop in mass-loss (relative to the results discussed in the previous section) is 0.9 dex for the 30 000 K models and 0.7 dex for the 40 000 K models. For the 30 000 K supergiant model, the increase in mass-loss due to the clumping effects discussed in Sect. 3.1 is essentially cancelled when porosity is also accounted for. In all other cases of this particular clumping stratification and clumping factor, the inclusion of porosity overcompensates for the effects of clumping on the photospheric radiation field and the ionization of the gas and causes a decrease in the mass loss relative to a smooth outflow. We note that for the smallest clump separation ($D = 1000$) the increase in $\dot{M}$ due to clumping effects alone is typically not fully compensated for by the porous nature of the medium. The mass-loss rate may go up, though not by more than a factor of three.

We note that for modest clumping ($C_c \leq 3$) the combined effects of clumping and porosity have a negligible effect when $D = 1000$; this leads to about a 20% decrease in $\dot{M}$ for $D = 100$,

while the mass-loss may drop by about a factor of two when $D = 10$.

4. Discussion

To discuss the effects of clumping and porosity on predicted values of the mass-loss rates of O-type stars and determine what the actual clumping factors should be in order to bring agreement between empirical and predicted mass-loss rates, we approximate the clumping and porosity effects on the predicted total kinetic energy $E_{\rm kin}$ by a power law. We thus assume that

$$E_{\rm kin}^{\rm pred}(C_{\rm c}) = C^{\alpha} \times E_{\rm kin}^{\rm pred}(C_{\rm c} = 1), \tag{12}$$

where the superscript "pred" represents prediction and $E_{\rm kin}(C_{\rm c} = 1)$ implies a homogeneous outflow. The typical uncertainty in this relation is 10 to 20 percent for the 30 000 K stars and less than 10 percent for the 40 000 K stars. Values of the power-law index α are given in Table 3 for the case in which clumping starts at the sonic point (model 2) and at 0.4 v_∞ (model 3) for different values of the porosity length, which are prescribed by the parameter D (see Eq. (7)).

Empirical mass-loss rates derived using the Hα line or the radio continuum may be affected by clumping because these diagnostics scale with the square of the density. Fits to these data assuming a homogeneous outflow should thus be corrected for clumping according to the relation

$$\dot{M}^{\rm emp}(C_{\rm c}) = C_{\rm c}^{-1/2} \times \dot{M}^{\rm emp}(C_{\rm c} = 1), \tag{13}$$

where the superscript "emp" represents empirical. To facilitate comparison, we assume that in the models where clumping develops near the sonic point, clumping predominantly impacts the mass-loss rate. If clumping sets in further out in the wind (at, say, 0.4 v_∞), the dominant impact is on the terminal flow velocity and not on $\dot{M}$ (see Krtička et al. 2008). We therefore focus our discussion on the results that have been obtained for models in which clumping sets in at the sonic point. In doing so, we replace the term $E_{\rm kin}^{\rm pred}$ in Eq. (12) by $\dot{M}^{\rm pred}$. To match the empirical and predicted mass-loss rates of a wind affected by clumping and porosity, it should thus hold that

$$\log\left(\frac{\dot{M}^{\rm emp}(C_{\rm c} = 1)}{\dot{M}^{\rm pred}(C_{\rm c} = 1)}\right) = (\alpha + 0.5)\log C_{\rm c}. \tag{14}$$

4.1. Accounting for clumping in both empirical estimates and predictions of mass-loss rates

When comparing the empirical and predicted mass-loss rates of O-type stars brighter than 175 000 $L_\odot$ with strong winds ($\dot{M} \gtrsim 1{-}2 \times 10^{-7} M_\odot$ yr^{-1}), Mokiem et al. (2007) found that the empirical rates are consistently higher than the predicted rates. This implies that in principle a clumping factor (for given porosity length) can be found such that $\dot{M}^{\rm emp}(C_{\rm c})$ and $\dot{M}^{\rm pred}(C_{\rm c})$ agree *if* $\alpha > -0.5$. For smaller values of α, the drop in predicted mass-loss rate due to the effect of clumping and porosity is so severe that it can never be matched by correcting the empirical mass-loss rate for the effect of clumping. Our predictions show that this situation will occur if clumping develops relatively close to the surface (near the sonic point) for large clump separations $L(r) \gtrsim 0.1 H_\rho$ (or $D \lesssim 10$).

The offset between empirical and predicted mass-loss rates assuming homogeneous outflows, as determined by Mokiem et al. (2007), is +0.27 dex for Galactic stars (see the left panel of their Fig. 4). This value is derived by comparing the empirical and predicted modified wind momentum (MWM) relation at a luminosity $\log(L/L_\odot) = 5.75$, which is typical of the stars investigated by these authors. As the slopes of these MWM relations are almost identical, the choice of luminosity may in principle have a small effect on the derived offset. The offset of +0.27 dex in the mass-loss rate implies that a clumping of $C_{\rm c} \simeq 3.5$ is sufficient to account for the difference between $\dot{M}^{\rm emp}$ and $\dot{M}^{\rm pred}$ *assuming clumping has no effect on the predicted mass-loss rates*. If one does account for clumping and porosity effects in the theoretical values, the clumping that is required may increase up to $C_{\rm c} \sim 10$ when $D \sim 100$, but may be slightly lower ($C_{\rm c} \sim 2.5{-}3.5$) if $D \sim 1000$ as, on average, the derived α values are positive. For porosity lengths corresponding to $D \lesssim 100$, the required clumping factor will increase steeply.

4.2. Observational constraints on the number of clumps

In Sect. 2.2.2, we estimated that the number of clumps per wind flow-time that we assumed in our models is $\sim 200\, D^3$. We now consider whether there are any empirical constraints either in support of or contradicting the assumed clump sizes and numbers in our models. Only rather rough order-of-magnitude estimates can presently be made.

Lépine & Moffat (1999) monitored a number of Wolf-Rayet stars spectroscopically discovering line-profile variations, which were interpreted as a large number (more than 10^4) of randomly distributed, radially propagating, discrete wind emission elements. Another way to derive the number and spatial scales of clumps is by using linear polarimetry that provides information about the geometry of the innermost portions of the stellar wind. Davies et al. (2007) showed that to reproduce the observed level of polarization variability of the LBVs P Cygni and AG Car the winds should consist of $\sim 10^3$ clumps per wind flow-time.

Quantitative estimates of the typical number of clumps in O-type stars have not yet been made, though line-profile variations do point to the presence of structure in their winds as well (see e.g. Eversberg et al. 1998; Lépine & Moffat 2008). The origin of the clumps likely controls their number. Cantiello et al. (2009) recently suggested that wind clumping might be induced by subsurface convection induced by the iron opacity peak in massive stars, where the density scale height in the iron opacity zone is approximately a factor 10^2 larger in LBV than in O star models. If wind clumping in LBVs and O stars were indeed induced by this iron opacity peak, one would then expect a factor 10^2 more clumps per wind flow-time in O star than in LBV winds, which would bring us in the range of 10^5 clumps per wind flow-time for O stars. This appears to be consistent with values of D at the lower end ($D \sim 10$) of the range studied in our paper. As pointed out in Sect. 4.1, such a relatively modest number of clumps would lead to lower expected mass-loss rates making it difficult to reconcile empirical and predicted mass-loss rates for stars with dense winds.

4.3. The weak-wind problem

For luminosities below about 175 000 $L_\odot$, a comparison between empirical and predicted mass-loss rates shows a large discrepancy referred to as the "weak-wind problem": empirical mass-loss rates appear to be up to two orders of magnitude lower than the predicted rates. At the moment, the nature of this weak-wind problem eludes us; for a discussion we refer to e.g. Martins et al. (2004), Martins et al. (2005), de Koter (2006),

Table 2. Adopted model parameters together with predicted mass loss rates for two clumping stratifications and porosity descriptions.

$T_{\rm eff}$ (K)	R [$R_\odot$]	$\log L$ [$L_\odot$]	M [$M_\odot$]	v_∞ [km s^{-1}]	$\log C_{\rm c}$	$\log \dot{M}$ [$M_\odot$ yr^{-1}]					
						$C_{\rm c}$ from $v_{\rm s}$			$C_{\rm c}$ from 0.4 v_∞		
						D = 10	D = 100	D = 1000	D = 10	D = 100	D = 1000
Dwarfs											
30 000	6.6	4.50	12.9	2176	0.0	–7.67	–7.67	–7.67	–7.67	–7.67	–7.67
					0.5	–7.97	–7.71	–7.67	–7.84	–7.67	–7.65
					1.0	–8.20	–7.79	–7.67	–7.96	–7.67	–7.60
					1.5	–8.54	–7.86	–7.55	–8.06	–7.64	–7.45
					2.0	–8.95	–7.93	–7.36	–8.01	–7.54	–7.19
40 000	10.7	5.42	34.6	2585	0.0	–6.13	–6.13	–6.13	–6.13	–6.13	–6.13
					0.5	–6.46	–6.22	–6.19	–6.37	–6.16	–6.13
					1.0	–6.71	–6.27	–6.16	–6.52	–6.19	–6.10
					1.5	–7.01	–6.38	–6.14	–6.61	–6.24	–6.03
					2.0	–7.34	–6.52	–6.17	–6.64	–6.22	–5.94
Supergiants											
30 000	22.4	5.56	28.8	1506	0.0	–5.90	–5.90	–5.90	–5.90	–5.90	–5.90
					0.5	–6.26	–6.00	–5.96	–6.15	–5.98	–5.93
					1.0	–6.41	–5.97	–5.87	–6.28	–5.91	–5.81
					1.5	–6.63	–5.90	–5.67	–6.35	–5.81	–5.63
					2.0	–6.88	–5.91	–5.42	–6.27	–5.72	–5.38
40 000	19.1	5.93	58.1	2212	0.0	–5.22	–5.22	–5.22	–5.22	–5.22	–5.22
					0.5	–5.57	–5.36	–5.30	–5.51	–5.28	–5.26
					1.0	–5.79	–5.44	–5.35	–5.64	–5.32	–5.22
					1.5	–6.08	–5.57	–5.39	–5.77	–5.36	–5.18
					2.0	–6.43	–5.71	–5.41	–5.76	–5.36	–5.13

Notes. The scale of the clumps is given by H_ρ/D. The clumping laws are: clumping starts at the sonic point (i.e. $C_{\rm c}$ from $v_{\rm s}$) and clumping starts at 0.4 v_∞ (i.e. $C_{\rm c}$ up to $v_{\rm s}$). We again emphasize that the mass-loss rates given here have been calculated assuming that all of the change in wind energy benefits $\dot{M}$. However, e.g. in the case in which clumping and porosity set in at 0.4 v_∞ this is highly unlikely; most of the change contributes to v_∞.

Fullerton et al. (2006), Mokiem et al. (2007), and Puls et al. (2008). In the context of the current study, a possible explanation could be that the winds of relatively low luminosity O stars become extremely clumpy and porous. Estimating the magnitude of the weak-wind problem for stars of 100 000 $L_\odot$ at about a factor of 30 (see for instance the right panel of Fig. 1 in Mokiem et al. 2007), a clumping factor $C_{\rm c} \approx 500$ and porosity length $D \approx 10$ could bring empirical and predicted estimates into agreement. It is however unclear why preferentially in low density stellar winds, typically at $\dot{M} \lesssim 1\text{–}2 \times 10^{-7}\, M_\odot$ yr^{-1}, such extreme inhomogeneities would develop.

5. Conclusions

We have investigated effects of clumping and porosity on predictions of the wind energy of O-type dwarf and supergiant stars using a method that is based on Monte Carlo radiative transfer. These results can be viewed as an addition to prescriptions provided by Vink et al. (2000, 2001). For five heuristic clumping stratifications, we investigate the effects of a clumpy medium on the wind energy by means of induced changes in the (photospheric) radiation field and the excitation and ionization state of the gas throughout the wind. In addition, we have investigated the effect of porosity by introducing a prescription in which the clump size is expressed as a fraction of the local density scale height. Clumps of size H_ρ/D equal to 1/10th, 1/100th, and 1/1000th of H_ρ have been considered. Our main conclusions are:

1. The presence of optically thin clumps favors the recombination of the gas, which for the temperature range investigated (between 30 000 and 40 000 K) causes an increase in the line force, hence an increase in the mass-loss rate. The larger the clumping factor $C_{\rm c}$ and the closer the star is to the bi-stability jump (at $\sim$ 25 000 K), the stronger is the effect.
2. Accounting for porosity effects in the clumped medium and the (wavelength-dependent) optical depth of the clumps, the mass-loss rate is found to decrease simply because photons may travel in-between the clumps, avoiding interactions with the gas. For small clumps ($D \gtrsim 1000$), this effect is not very important, but for larger clumps ($D \lesssim 100$) the overall effect is a net decrease in $\dot{M}$.

Table 3. Fitted behavior of the effects of clumping and porosity when clumping sets in at the sonic point (model 2) and at 0.4 v_∞ (model 3).

D	30 000 V	40 000 V	30 000 I	40 000 I
clumping sets in at the sonic point (model 2)				
10	–0.61	–0.59	–0.50	–0.60
100	–0.13	–0.18	–0.02	–0.24
1000	+0.11	–0.02	+0.17	–0.11
∞	+0.26	+0.19	+0.43	+0.10
clumping sets in at 0.4v_∞ (model 3)				
10	–0.22	–0.30	–0.26	–0.33
100	+0.04	–0.06	+0.06	–0.08
1000	+0.19	+0.08	+0.20	+0.03
∞	+0.24	+0.21	+0.40	+0.20

Notes. The total kinetic energy is fitted to the function $E_{\rm kin} = E_{\rm kin}(C_{\rm c} = 1) \times C_{\rm c}^{\alpha}$, for each type of star and clump separation $L(r) = H_\rho(r)/D$. For given values of D, the table lists the values of α. $D = \infty$, corresponds to non-porous models

3. For clump sizes corresponding to $D \sim 100$ or larger, the net effect on $\dot{M}$ is small. Assuming that the velocity structure is not affected by clumps, the mass-loss rate decreases by less than a factor of two, even for clumping factors $C_c \sim 100$. For large clumps, corresponding to $D \lesssim 10$, the effect is more dramatic. Already for modest clumping, we find that $\dot{M} \propto C_c^{\alpha}$ with $\alpha \sim -0.5$ to -0.6. For such a steep dependence, empirical mass-loss rates based on Hα measurements, which are found to be about a factor of two higher than predictions assuming smooth outflows, can no longer be reconciled with theoretical $\dot{M}$ values by applying clumping corrections.
4. Though large clumps and very large clumping factors may dramatically reduce the mass-loss rate, the occurrence of this type of structure is not likely the explanation of the "weak-wind problem" for stars with $L \lesssim 10^{5.2}\ L_{\odot}$, unless a mechanism can be identified that causes extreme structure to develop in winds of $\dot{M} \lesssim 1{-}2 \times 10^{-7}\ M_{\odot}\ \mathrm{yr}^{-1}$ that is not active in denser winds.

Acknowledgements. We would like to thank Joachim Puls for suggestions on how to verify the implementation of clumping and constructive discussions. J.K. and J.K. kindly acknowledge support from grant GA ČR 205/08/0003.

References

Abbott, D. C., & Lucy, L. B. 1985, ApJ, 288, 679
Anders, E., & Grevesse, N. 1989, Geochim. Cosmochim. Acta, 53, 197
Asplund, M., Grevesse, N., & Sauval, A. J. 2005, in Cosmic Abundances as Records of Stellar Evolution and Nucleosynthesis, ed. T. G. Barnes, III & F. N. Bash, ASP Conf. Ser., 336, 25
Bouret, J., Lanz, T., Hillier, D. J., et al. 2003, ApJ, 595, 1182
Bouret, J., Lanz, T., & Hillier, D. J. 2005, A&A, 438, 301
Cantiello, M., Langer, N., Brott, I., et al. 2009, A&A, 499, 279
Crowther, P. A., Hillier, D. J., Evans, C. J., et al. 2002, ApJ, 579, 774
Davies, B., Vink, J. S., & Oudmaijer, R. D. 2007, A&A, 469, 1045
de Koter, A. 2006, in Stellar Evolution at Low Metallicity: Mass Loss, Explosions, Cosmology, ed. H. J. G. L. M. Lamers, N. Langer, T. Nugis, & K. Annuk, ASP Conf. Ser., 353, 99
de Koter, A., Schmutz, W., & Lamers, H. J. G. L. M. 1993, A&A, 277, 561
de Koter, A., Heap, S. R., & Hubeny, I. 1997, ApJ, 477, 792
de Koter, A., Vink, J. S., & Muijres, L. 2008, in Clumping in Hot-Star Winds, ed. W.-R. Hamann, A. Feldmeier, & L. M. Oskinova, 47
Dessart, L., & Owocki, S. P. 2003, A&A, 406, L1
Dessart, L., & Owocki, S. P. 2005, A&A, 437, 657
Eversberg, T., Lepine, S., & Moffat, A. F. J. 1998, ApJ, 494, 799
Feldmeier, A. 1995, A&A, 299, 523
Feldmeier, A. 1999, in Lecture Notes in Physics, Variable and Non-spherical Stellar Winds in Luminous Hot Stars, IAU Colloq. 169, ed. B. Wolf, O. Stahl, & A. W. Fullerton (Berlin: Springer Verlag) 523, 285
Feldmeier, A., Oskinova, L., & Hamann, W. 2003, A&A, 403, 217
Figer, D. F., Najarro, F., Gilmore, D., et al. 2002, ApJ, 581, 258
Fullerton, A. W., Massa, D. L., & Prinja, R. K. 2006, ApJ, 637, 1025
Gräfener, G., & Hamann, W. 2008, A&A, 482, 945
Hillier, D. J. 1991, A&A, 247, 455
Hillier, D. J., Lanz, T., Heap, S. R., et al. 2003, ApJ, 588, 1039
Krtička, J., & Kubát, J. 2007, A&A, 464, L17
Krtička, J., Puls, J., & Kubát, J. 2008, in Clumping in Hot-Star Winds, ed. W.-R. Hamann, A. Feldmeier, & L. M. Oskinova, 111
Lépine, S., & Moffat, A. F. J. 1999, ApJ, 514, 909
Lépine, S., & Moffat, A. F. J. 2008, AJ, 136, 548
Lucy, L. B., & Solomon, P. M. 1970, ApJ, 159, 879
Markova, N., Puls, J., Repolust, T., & Markov, H. 2004, A&A, 413, 693
Martins, F., Schaerer, D., Hillier, D. J., & Heydari-Malayeri, M. 2004, A&A, 420, 1087
Martins, F., Schaerer, D., Hillier, D. J., et al. 2005, A&A, 441, 735
Mokiem, M. R., de Koter, A., Vink, J. S., et al. 2007, A&A, 473, 603
Muijres, L., Vink, J. S., de Koter, A. et al. 2010, A&A, submitted
Müller, P. E., & Vink, J. S. 2008, A&A, 492, 493
Oskinova, L. M., Hamann, W.-R., & Feldmeier, A. 2007, A&A, 476, 1331
Owocki, S. P. 1994, Ap&SS, 221, 3
Owocki, S. P. 2008, in Clumping in Hot-Star Winds, ed. W.-R. Hamann, A. Feldmeier, & L. M. Oskinova, 121
Owocki, S. P., & Puls, J. 1996, ApJ, 462, 894
Owocki, S. P., & Puls, J. 1999, ApJ, 510, 355
Owocki, S. P., & Cohen, D. H. 2006, ApJ, 648, 565
Owocki, S. P., Castor, J. I., & Rybicki, G. B. 1988, ApJ, 335, 914
Owocki, S. P., Gayley, K. G., & Shaviv, N. J. 2004, ApJ, 616, 525
Puls, J., Springmann, U., & Owocki, S. P. 1998, in Cyclical Variability in Stellar Winds, ed. L. Kaper & A. W. Fullerton, 389
Puls, J., Markova, N., Scuderi, S., et al. I. D. 2006, A&A, 454, 625
Puls, J., Vink, J. S., & Najarro, F. 2008, A&ARv, 16, 209
Repolust, T., Puls, J., & Herrero, A. 2004, A&A, 415, 349
Runacres, M. C., & Owocki, S. P. 2002, A&A, 381, 1015
Runacres, M. C., & Owocki, S. P. 2005, A&A, 429, 323
Sobolev, V. V. 1960, Moving envelopes of stars, ed. V. V. Sobolev
Sundqvist, J. O., Puls, J., & Feldmeier, A. 2010, A&A, 510, A11
Vink, J. S., & de Koter, A. 2002, A&A, 393, 543
Vink, J. S., & de Koter, A. 2005, A&A, 442, 587
Vink, J. S., de Koter, A., & Lamers, H. J. G. L. M. 1999, A&A, 350, 181
Vink, J. S., de Koter, A., & Lamers, H. J. G. L. M. 2000, A&A, 362, 295
Vink, J. S., de Koter, A., & Lamers, H. J. G. L. M. 2001, A&A, 369, 574